248, 2621 (1973); P. Hausen and H. Stein, *Eur. J. Biochem.* **14**, 278 (1970); H. Donis-Keller, *Nucleic Acids Res.* **7**, 179 (1979).
21. D. Baltimore, *Nature* **226**, 1209 (1970); H. M. Temin and S. Mizutani, *ibid.*, p. 1211; L. A. Kohlstaedt, J. Wang, J. M. Friedman, P. A. Rice, T. A. Steitz, *Science* **256**, 1783 (1992).
22. The CD experiments were performed on an Aviv model 60 spectrophotometer with thermostatically controlled cell holder (path length = 10 mm). The spectra displayed are the average of three scans taken at 25°C minus the averaged spectra of the buffer alone. Samples were prepared at 2 μM concentration in each strand and annealed in buffer containing 100 mM NaCl, 10 mM sodium cacodylate-cacodylic acid, pH 5.5, and 1 mM EDTA.
23. We thank K. Harris, who was instrumental in the early stages of this work, J. Flory for synthesis of RNA and hybrid duplex sites, and G. Sun for synthesis of RNA and all DNA samples and templates. This work was supported by NIH grant Gar 21966.

15 July 1992; accepted 9 October 1992

# Simultaneous Miocene Extension and Shortening in the Himalayan Orogen

K. V. Hodges,* R. R. Parrish, T. B. Housh, D. R. Lux, B. C. Burchfiel, L. H. Royden, Z. Chen

**The South Tibetan detachment system separates the high-grade metamorphic core of the Himalayan orogen from its weakly metamorphosed suprastructure. It is thought to have developed in response to differences in gravitational potential energy produced by crustal thickening across the mountain front. Geochronologic data from the Rongbuk Valley, north of Qomolangma (Mount Everest) in southern Tibet, demonstrate that at least one segment of the detachment system was active between 19 and 22 million years ago, an interval characterized by large-scale crustal thickening at lower structural levels. These data suggest that decoupling between an extending upper crust and a converging lower crust was an important aspect of Himalayan tectonics in Miocene time.**

Although the Himalayan orogen is the product of continent-continent collisional tectonics, the Late Miocene to Recent tectonic evolution of Tibet has been characterized by east-west extension (*1–3*). This extension has been attributed to the collapse of the Tibetan Plateau as a result of body forces arising from crustal thickness contrasts between the plateau and its surroundings (*4, 5*). It is commonly assumed that gravitational collapse characterizes the latest stages in the evolution of a compressional mountain belt (*6, 7*), which correspond to a time when convergence across the orogen slows dramatically or ceases. In the case of Tibet, Mercier and co-workers (*3*) suggested that the onset of east-west extension in Late Miocene time marked a fundamental change from a compressional to an extensional regime. However, recent studies of the southern margin of the Tibetan Plateau have led to the identification of a major set of extensional structures (the South Tibetan detachment system, or STDS) that developed before Late Miocene extension (*8, 9*). Here, we present geochronologic data that closely constrain the age of one segment of the STDS north of Qomolangma (Mount Everest or Sagarmatha) and imply that the detachment system was active synchronously with thrusting at deeper structural levels. The documentation of coeval, large-scale thrust and normal faulting in the Himalayas has important implications for the understanding of the dynamics of collisional orogenesis.

The metamorphic core of the Himalayan orogen (Fig. 1) consists predominately of amphibolite facies schists and gneisses of the Greater Himalayan metamorphic sequence (*10, 11*). This package of rocks is bound below by the moderately northward-dipping Main Central thrust (MCT) system. This system, which accommodated a significant proportion (>100 km) of shortening across the orogen (*11*), has had a long and complex history. In some transects [for example, the Manaslu region of central Nepal (*12*)], most of the displacement on the MCT system appears to have taken place at upper greenschist facies to amphibolite facies conditions during Miocene regional metamorphism. In other areas [the Langtang region north of Kathmandu (*13*)], a significant amount of displacement occurred at lower greenschist facies conditions as late as Pliocene time. Some of the best constraints on the age of early, high-temperature movement on the MCT system come from the area south of Qomolangma. Here, the MCT corresponds to a 3- to 5-km-thick mylonite zone developed at temperatures ranging from 770 to 1000 K (500° to 730°C) (*14*). Hornblende from an amphibolite collected in the lower MCT zone yielded a $^{40}Ar/^{39}Ar$ isochron age of 20.9 ± 0.4 Ma (million years ago) (*15*). Given that deformation in this part of the shear zone took place at temperatures close to the closure temperature for Ar diffusion in metamorphic amphibole (*16, 17*), Hubbard and Harrison (*15*) interpreted the 20.9 Ma date as the approximate age of movement on the MCT at the longitude of Qomolangma.

The Greater Himalayan sequence is separated from structurally higher miogeoclinal strata of the Tibetan sedimentary sequence by north-dipping extensional structures of the STDS (Fig. 1). The STDS spans a distance of greater than 1000 km between northwest India and Bhutan (*8, 9, 18, 19*). At the longitude of Qomolangma, the principal structure of the STDS is the Qomolangma detachment, a brittle normal fault that dips between 5° and 15° to the northeast and is marked by a 3- to 10-m-wide zone of fault breccias. We have mapped this detachment and related structures in the Rongbuk Valley (Fig. 2), due north of Qomolangma (*9*).

The hanging wall of the Qomolangma detachment includes weakly metamorphosed Ordovician limestone, calcareous shale, and siltstone that corresponds to the Tibetan sedimentary sequence. The footwall, representing the Greater Himalayan sequence, is an amphibolite facies injection complex that consists of intercalated calc-silicate gneiss, marble, amphibolite, and pelitic to psammitic schist, all of which are intruded by multiple generations of leucogranitic dikes and sills. The predominant fabric in the injection complex is a northwest-striking, axial planar schistosity ($S_1$) that was penecontemporaneous with the growth of early metamorphic porphyroblasts. Within 500 m of the Qomolangma detachment, $S_1$ is overprinted by S-C mylonitic fabrics assigned to a second stage of deformation ($D_2$). The principal shear planes in this mylonite dip shallowly northward, subparallel to the detachment, and fabric asymmetries indicate that the mylonite represents a normal-sense shear zone. We interpret this shear zone as an early manifestation of the Qomolangma detachment that developed at relatively deep crustal levels and was subsequently transported to the upper crust by continued normal-sense movement on the detachment system. Well-developed stretching and mineral lineations in the mylonites plunge shallowly at N15° to 35°E, suborthogonal to the strike of small, rotated fault blocks developed during brittle movement on the detachment system. Consequently, we infer that displacement on the Qomolangma de-

K. V. Hodges, T. B. Housh, B. C. Burchfiel, L. H. Royden, Department of Earth, Atmospheric, and Planetary Sciences, Massachusetts Institute of Technology, Cambridge, MA 02139.
R. R. Parrish, Geological Survey of Canada, Ottawa, Ontario K1A 0E8, Canada.
D. R. Lux, Department of Geology, University of Maine, Orono, ME 04469.
Z. Chen, Chengdu Institute of Geology and Mineral Resources, Chengdu 610082, Sichuan, China.
*To whom correspondence should be addressed.

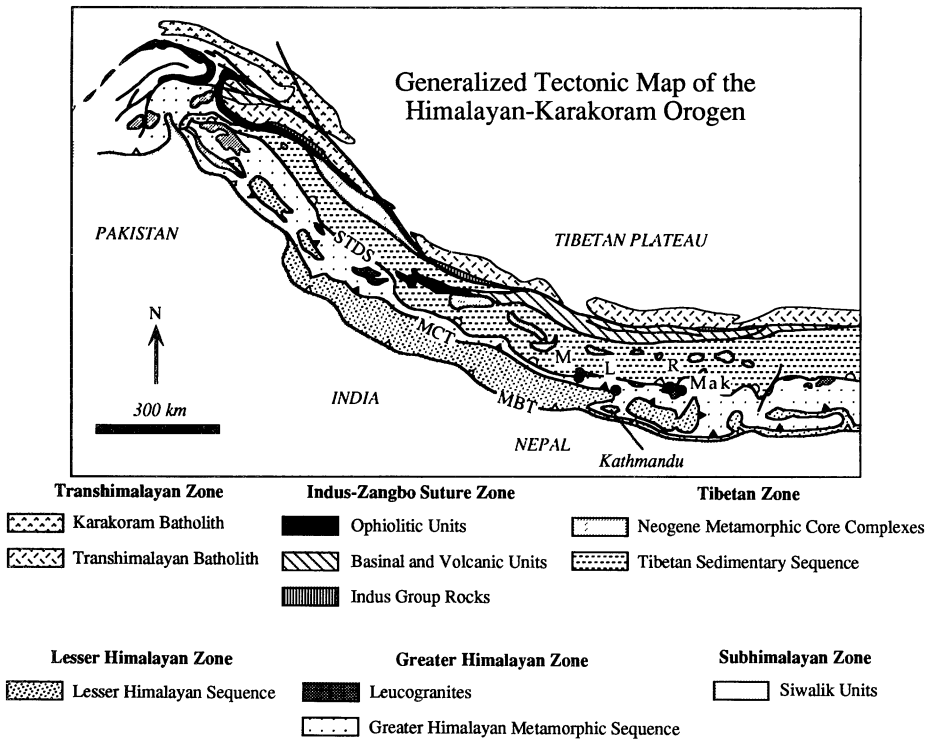


**Fig. 1.** Generalized tectonic map of the Himalayan-Karakoram orogen. Major fault systems include the South Tibetan detachment system (STDS), the Main Central thrust system (MCT), and the Main Boundary thrust system (MBT). Filled circles indicate locations of the Manaslu (M), Langtang (L), Rongbuk Valley (R), and Makalu (Mak) regions.

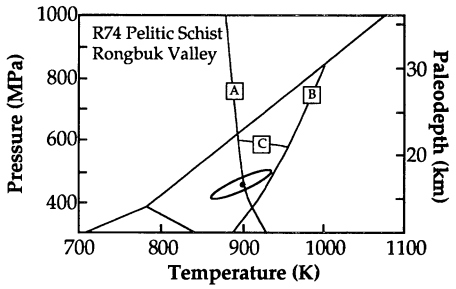


**Fig. 3.** Thermobarometric results for sample R74. Small, filled circle indicates PT conditions derived through simultaneous solution of the garnet-biotite and garnet-plagioclase-sillimanite-quartz thermobarometers, and the ellipse corresponds to $2\sigma$ precision limits based on analytical uncertainties (*20*). Unlabeled thin curves separate the aluminum silicate stability fields (*35*). A, water-saturated granite solidus (*36*); B, nominal muscovite breakdown reaction (*36*); C, upper pressure stability limit for magmatic cordierite in peraluminous granitic melts (*37, 38*).

tachment system was toward the north-northeast throughout its history.

Mineral assemblages observed in the injection complex (sillimanite ± muscovite ± K-feldspar in pelitic rocks) indicate that upper amphibolite facies metamorphic conditions accompanied $D_1$ and $D_2$. Low-variance mineral assemblages suitable for quantitative thermobarometry are relatively rare in Rongbuk Valley, but we did find one pelitic schist sample (R74; Fig. 2) with an appropriate mineralogy for simultaneous solution of the garnet-biotite and garnet-plagioclase-sillimanite-quartz thermobarometers. We calculated final equilibration conditions of 900 K (630°C) and 460 MPa (4.6 kbar) for this sample (*20, 21*). Calculated pressure-temperature (PT) conditions are consistent with field evidence of widespread anatectic melting and with petrographic observations of cordierite as well as sillimanite and muscovite in rocks from this part of the injection complex (Fig. 3). Given the possibility of reequilibration during cooling in these high-grade rocks (*22*), we interpret the R74 PT data as evidence of temperatures at least as high as 900 K (630°C) at depths of about 17 km during metamorphism.

At least two generations of leucogranites occur in the Rongbuk Valley. The oldest granites are restricted to the injection complex and contain the assemblage quartz + K-feldspar + plagioclase + muscovite + tourmaline ± biotite ± garnet ± sillimanite. These granites form concordant sills up to 100 m thick and are strongly mylonitized in the shear zone beneath the Qomolangma detachment. The youngest granites are biotite-poor, contain cordierite, and are much less common than the older granites. They generally occur as small (up to 1 m thick), unfoliated dikes, but there is one relatively large body of late leucogranite exposed on the east wall of Rongbuk Valley and referred to hereafter as the Rongbuk pluton. Unlike the older granites, the youngest suite cuts across all structures and fabrics in the injection complex. More significantly, the Rongbuk pluton intrudes the Qomolangma detachment and has produced a narrow (~10 to 50 m wide), high-temperature contact aureole in carbonate rocks of the Tibetan sedimentary sequence (Fig. 2).

The Qomolangma detachment marks an

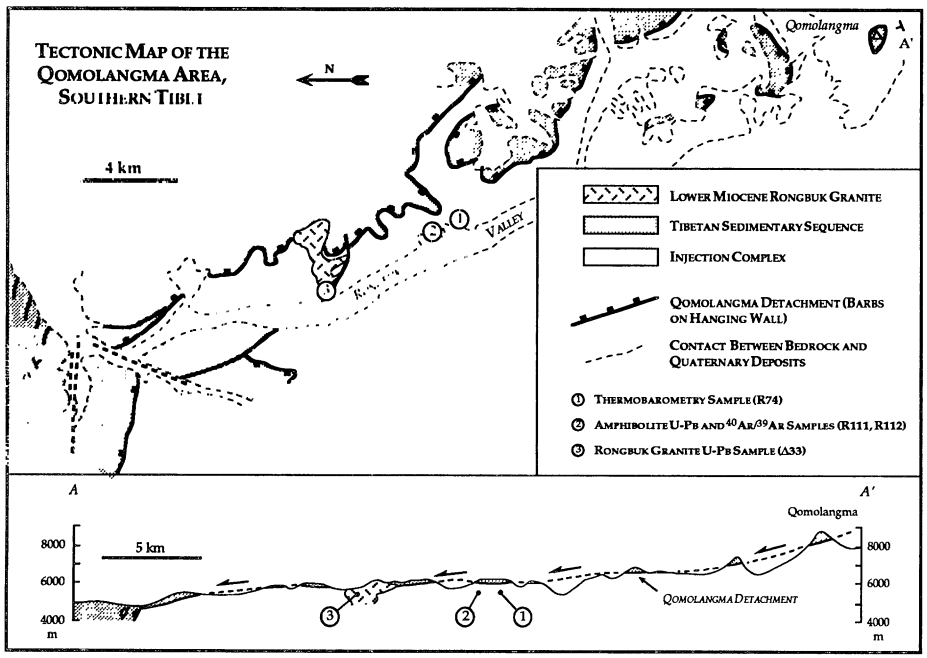


**Fig. 2.** Generalized tectonic map and cross section of Rongbuk Valley, adapted from (*9*).

abrupt discontinuity between weakly metamorphosed rocks of the Tibetan sedimentary sequence and upper amphibolite facies rocks of the injection complex. Although textural relations indicate that the early stages of movement on the $D_2$ shear zone beneath the detachment occurred at relatively high temperatures, most of the displacement on the Qomolangma detachment must postdate metamorphism in the injection complex. The cross-cutting Rongbuk pluton provides a minimum age constraint on the structure.

We have used a combination of U-Pb and $^{40}Ar/^{39}Ar$ geochronology to constrain the age of sillimanite-grade metamorphism at a structural level roughly 600 m below the detachment (samples R111 and R112; Fig. 2). This locality lies below the $D_2$ shear zone and roughly 4 km south of the Rongbuk pluton, well outside the contact aureole of the late granite. Samples R111 and R112 were collected from a concordant amphibolitic schist body and contain the assemblage hornblende + plagioclase + biotite + quartz + titanite. A hand-picked, high-purity aliquot of titanite was separated from sample R111 and analyzed for U-Pb geochronology at the Massachusetts Institute of Technology (Table 1 and Fig. 4) (*23*). As is commonly the case for titanite, the Pb in this sample was not very radiogenic, and the common Pb correction is significant. In order to better estimate initial Pb isotopic compositions, we analyzed the residue of HF-leached plagioclase separated from R111 and assumed that the plagioclase and titanite were in Pb isotopic equilibrium at the time of metamorphism. Errors in this common Pb correction would result in a shift of the plotting coordinates for the sample roughly parallel to the $^{207}Pb/^{235}U$ axis in Fig. 4. We conclude that the $^{206}Pb/^{238}U$ age obtained for the titanite (20.3 ± 0.1 Ma) is the best estimate of the time of cooling of sample R111 through the nominal closure temperature for Pb diffusion in titanite. Estimates of this temperature have ranged from 770 to 940 K (500° to 670°C) (*17*, *24–27*). The most recent work of Mezger and co-workers (*27*) suggests that the closure temperature of titanite is strongly dependent on physical grain size; for the sizes encountered in R111 (~0.5 cm) and a reasonable cooling rate between 10 and 100 K per million years, an estimate in the range 870 to 910 K (600° to 640°C) seems appropriate.

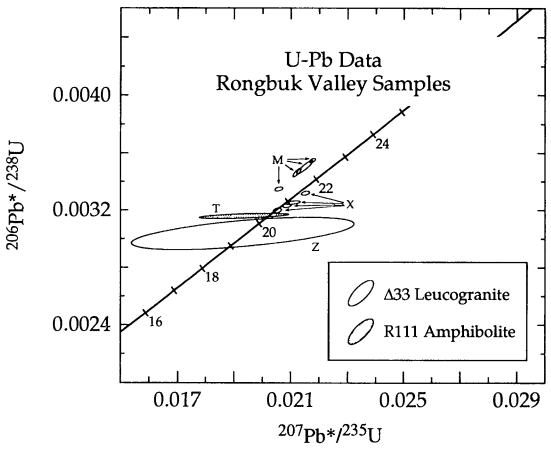


**Fig. 4.** U-Pb concordia plot for samples from Rongbuk Valley. Ellipses correspond to 2σ precision limits. M, monazite; T, titanite; X, xenotime; Z, zircon. Data for Δ33 monazite and zircon are from (*29*).

Hornblende separates from R111 and R112 were analyzed with the use of the $^{40}Ar/^{39}Ar$ mass spectrometry facilities at the University of Maine (Fig. 5) (*28*). Sample R112 yielded a slightly saddle-shaped release spectrum suggestive of incorporation of "excess" or unsupported radiogenic $^{40}Ar$ at the time of hornblende crystallization (*16*). Consequently, our best estimate of the minimum closure age of this sample is the minimum age on the release spectrum: 19.1 Ma. Sample R111 was much better behaved during the incremental heating experiment; despite evidence of excess radiogenic $^{40}Ar$ in the earliest steps, over 97% of the gas in this sample yielded a plateau age of 20.0 ± 0.9 Ma. We interpret this age, which is consistent with the minimum age for R112, as the time of cooling of the R111-R112 sample locality through the nominal Ar closure temperature for hornblende: 780 to 810 K (510° to 540°C) for a cooling rate between 10 and 100 K per million years (*16*, *17*). Noting that the hornblende from R111 yields a plateau age indistinguishable from the $^{206}Pb/^{238}U$ age of titanite from the same sample, we conclude that this structural horizon experienced rapid cooling (~100 K per million years) at roughly 20 Ma. Given this cooling rate and that the probable closure temperature of the R111 titanites was not significantly different from the thermobarometric temperature estimates obtained for R74, it seems probable that the injection complex in Rongbuk Valley was experiencing upper amphibolite-facies PT conditions as recently as 21 Ma.

The U-Pb systematics of accessory minerals in the Rongbuk leucogranite are exceedingly complex. Copeland and co-workers (*29*) demonstrated that most zircons and monazites from sample Δ33 (Fig. 2) contain a component of inherited radiogenic Pb. The youngest monazite fractions plot above the concordia [a common occurrence in monazites, which indicates excess $^{206}Pb$ that is probably derived from $^{230}Th$ incorporated into the structure during crystallization (*30*)] and yield $^{207}Pb/^{235}U$ ages of 21 to 22 Ma. One crystal of igneous zircon provided a concordant but relatively imprecise date of 19.5 ± 0.4 Ma (Fig. 4).

In an effort to constrain the crystallization age of the pluton better, we analyzed four xenotime separates from Δ33 at the Geological Survey of Canada laboratory in Ottawa (Table 1 and Fig. 4) (*31*). All but one of the xenotime ages are concordant within analytical uncertainty, with apparent ages ranging from 20.6 to 21.6 Ma. The spread of xenotime ages is roughly equiva-

**Table 1.** U-Pb data for samples from Rongbuk Valley, Tibet. Age uncertainties are reported at the 95% confidence level. For the titanite sample, initial Pb was assumed to be that measured for plagioclase from sample R111. For xenotimes, initial Pb is assumed with the use of the Stacey and Kramers Pb evolution model (*39*).

| Sample | Weight (mg) | U (ppm) | Pb (ppm) | $^{206}Pb/^{204}Pb^*$ | $^{208}Pb\dagger/^{206}Pb\dagger$ | $^{206}Pb\dagger/^{238}U$ | $^{207}Pb\dagger/^{235}U$ | $^{206}Pb/^{238}U$ age (Ma) | $^{207}Pb/^{235}U$ age (Ma) |
|---|---|---|---|---|---|---|---|---|---|
| | | | | | *Titanite* | | | | |
| R111 | 19.7 | 63.1 | 2 83 | 23.60 | 0.101 | 0.00316 | 0.01934 | 20.3 ± 0.1 | 19.5 ± 1.3 |
| | | | | | *Xenotime* | | | | |
| Δ33A | 0.0389 | 17,299 | 52.77 | 3,095 | 0.060 | 0.00320 | 0.02053 | 20.6 ± 0.1 | 20.6 ± 0.1 |
| Δ33B | 0.0238 | 19,474 | 61.10 | 1,903 | 0.042 | 0.00333 | 0.02149 | 21.4 ± 0 1 | 21.6 ± 0.1 |
| Δ33C | 0.0290 | 8,248 | 26.24 | 599 | 0.068 | 0.00326 | 0.02106 | 21.0 ± 0.1 | 21.2 ± 0.2 |
| Δ33D | 0.0236 | 20,481 | 62.75 | 1,316 | 0.045 | 0.00323 | 0.02085 | 20.8 ± 0.1 | 21.0 ± 0.1 |

*Measured ratio, corrected for mass fractionation and blank. †Radiogenic component, corrected for mass fractionation, blank, and initial Pb

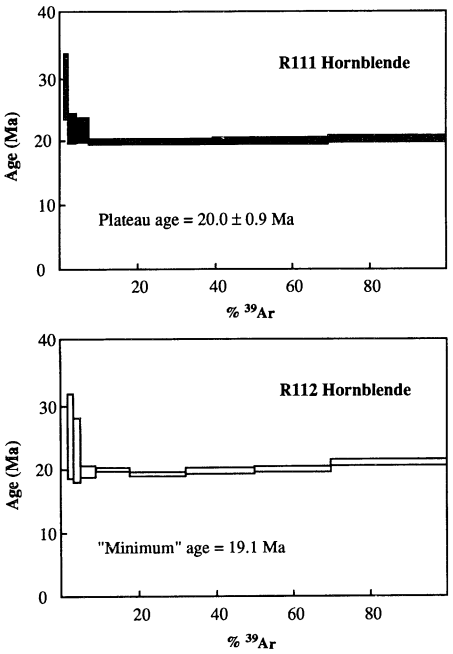


**Fig. 5.** $^{40}Ar/^{39}Ar$ release spectra for hornblendes from samples R111 and R112. For the sake of clarity, the first three increments of the R111 experiment and the first two increments of the R112 experiment have been omitted from the diagram. The last six increments for R111 (filled) are consistent within analytical uncertainty and define a plateau age of 20.0 ± 0.9 Ma.

lent to that found for young monazites from this sample and somewhat older than the single magmatic zircon studied by Copeland and co-workers (*29*). Similar variations in concordant and near-concordant U-Pb ages of apparently magmatic accessory minerals have been reported from other Himalayan leucogranites (*30, 32, 33*). We see three possible explanations for the Rongbuk pluton xenotime behavior. It could represent postcrystallization Pb loss from some of the xenotimes, which implies that the actual crystallization age of the pluton is at least as old as 21.6 Ma. Alternatively, the age spread could represent episodic crystallization of xenotime over the 21.6 to 20.6 Ma interval, which suggests a duration of ~1 million years for the magmatic evolution of the Rongbuk pluton. However, both of these interpretations are inconsistent with field relations that indicate that the pluton postdates the ~21 Ma amphibolite facies metamorphism of the injection complex. Given the evidence for inheritance of both monazite and zircon in Δ33, it is possible that the spread of xenotime ages reflects mixing between a young (~19.5 Ma) magmatic component and an older, inherited component. The data array in Fig. 4 suggests that the older xenotime component, if it exists, must have a relatively young (Cenozoic) age. One possible source of xenocrystic xenotime is the older leucogranite suite in the injection complex. We note that the Makalu pluton, an early leucogranite body exposed a few tens of kilometers southeast of Qomolangma and perhaps coeval with the early granite suite in Rongbuk Valley, has yielded concordant xenotime ages as great as 23.5 Ma (*30*). Further assessment of this hypothesis must await U-Pb studies on the older leucogranites in Rongbuk Valley. For now, we adopt the interpretation that the crystallization age of the Rongbuk pluton is between 21.6 and 19.5 Ma.

Within analytical uncertainty, the age of amphibolite-facies metamorphism in the injection complex of Rongbuk Valley is the same as the intrusive age of the Rongbuk pluton. The simplest and most conservative interpretation of the geochronologic and field data regarding the Qomolangma detachment is that all of the fault movement and most (if not all) of the $D_2$ mylonitization occurred between 22 and 19 Ma. A younger age would require the improbable case that all concordant mineral ages for the cross-cutting Rongbuk pluton are a result of inheritance. An older age would imply the emplacement of hanging wall strata when the injection complex was still at temperatures of 780 to 910 K (510° to 640°C), a range that encompasses all probable closure temperatures for Ar in hornblende and Pb in titanite. This seems unlikely, given the preservation of delicate fossils and sedimentary structures in the Tibetan sedimentary sequence and the lack of petrographic evidence in these rocks for anything other than very low grade to low-grade metamorphism (*9*). It could be argued that the similarity in ages between R111, R112, and Δ33 minerals suggests that the heating during intrusion of the Rongbuk pluton was sufficient to reset the isotopic "clocks" in R111 and R112 and that the true age of regional metamorphism is much greater than 22 Ma. This scenario seems improbable because a substantial influx of heat for a protracted period would be required to induce significant Pb loss from the R111 titanites, and the pluton is neither sufficiently large nor sufficiently close to the R111 locality to have had much of a thermal effect.

Accepting an age of 22 to 19 Ma for the Qomolangma detachment permits us to constrain the displacement rate on the fault. The cross section in Fig. 2 strikes roughly parallel to the inferred movement direction on the fault. Note that the detachment can be traced nearly continuously from the north end of Rongbuk Valley to the top of Qomolangma, and nowhere along this transect can we match hanging wall and footwall lithologic units. This observation implies a minimum of 34 km of displacement. All of this movement must have taken place in 3 million years or less, requiring a minimum average slip rate of roughly 1.1 cm/year. Using an approximate average dip of 10° for the detachment (*9*), we calculated that the minimum amount of unroofing of the injection complex resulting from movement on the detachment was 6 km and that the minimum average unroofing rate would have been roughly 2 mm/year. Numerical experiments suggest that the thermal significance of tectonic unroofing on normal fault systems is proportional to the rate of displacement (*34*); given the slip rate suggested by the data presented here, it seems inescapable that the Qomolangma detachment had an important impact on the thermal evolution of the Greater Himalayan sequence.

Recalling the 20.9-Ma age assigned by Hubbard and Harrison (*15*) to the MCT south of Qomolangma, we note that all of the available geologic data are consistent with contemporaneous movement of the MCT and STDS at this longitude. The geologic record and historic seismicity clearly show that compressional deformation has occurred in the Himalayan orogen since displacement on the Qomolangma detachment. We infer that extension related to gravitational collapse is not restricted to the final stages of mountain building but instead is a fundamental part of compressional orogenesis that may recur with some frequency as compressional and gravitational forces compete for control of the orogenic profile.

## REFERENCES AND NOTES


1. P. Molnar and P. Tapponnier, *J Geophys. Res.* **83**, 5361 (1978).
2. R. Armijo, P. Tapponnier, J. Mercier, T. Han, *ibid.* **91**, 13803 (1986).
3. J.-L. Mercier, R Armijo, P. Tapponnier, E. Carey-Gailhardis, T. L. Han, *Tectonics* **6**, 275 (1987).
4. P. Tapponnier and P. Molnar, *Nature* **264**, 319 (1976).
5. P. England and G. Houseman, *J Geophys. Res.* **94**, 17561 (1989)
6. L. J Sonder, P. C. England, B. P. Wernicke, R. L. Christiansen, in *Continental Extensional Tectonics*, M. P. Coward, J. F. Dewey, P. L. Hancock, Eds. (Spec. Publ. 28, Geological Society of London, Oxford, 1987), pp. 187–201
7. J. F. Dewey, *Tectonics* **7**, 1123 (1988)
8. J. P. Burg and G. M. Chen, *Nature* **311**, 219 (1984).
9. B. C. Burchfiel *et al.*, *Geol. Soc. Am. Spec. Pap. 269* (1992).
10. A Gansser, *Geology of the Himalayas* (Wiley Interscience, London, 1964).
11. P. LeFort, *Am. J. Sci.* **275A**, 1 (1975).
12. A. Pêcher, thesis, University of Grenoble (1978).
13. A. M. Macfarlane, thesis, Massachusetts Institute of Technology (1992).
14. M S Hubbard, *J. Metamorph Geol.* **7**, 19 (1989)
15. _____ and T M Harrison, *Tectonics* **8**, 865 (1989). Here and throughout the paper, age uncertainties are reported at the 2σ confidence level.
16. I McDougall and T M Harrison, *Geochronology and Thermochronology by the $^{40}Ar/^{39}Ar$ Method* (Oxford Univ. Press, New York, 1988).

17. K. V. Hodges, *Annu. Rev. Earth Planet. Sci.* **19**, 207 (1991).
18. E. Herren, *Geology* **15**, 409 (1987).
19. A. Pêcher, *Tectonics* **10**, 587 (1991).
20. K. V. Hodges and L. W. McKenna, *Am. Mineral.* **72**, 671 (1987).
21. For information concerning analytical techniques, see Hodges and McKenna (*20*). We adopted the calibration of Hodges and McKenna for the garnet-biotite thermometer and that of L. W. McKenna and K. V. Hodges [*ibid.* **73**, 1205 (1988)] for the garnet-plagioclase-sillimanite-quartz barometer. Nonideal solution behavior was modeled for garnet [R. G. Berman, *ibid.* **75**, 328 (1990)] and for plagioclase (L. T. Elkins and T. L. Grove, *ibid.*, p. 544).
22. F. S. Spear and F. Florence, *J. Metamorph. Geol.* **9**, 379 (1991).
23. Analyses were done with the use of a VG Sector 54 mass spectrometer (Fisons Instruments, Danvers, MA) in static multicollector mode. The titanite was dissolved in a mixture of 0.5 ml of 6 N HCl and 0.1 ml of HF at 450 K (~175°C). Pb and U were separated with the use of HBr media and $HNO_3$-media anion exchange chemistry, respectively. Pb was loaded with silica gel and $H_3PO_4$ on a Re filament, whereas U was loaded on Re with the use of $H_3PO_4$ and colloidal graphite and run as a metal
24. J. M. Mattinson, *Contrib. Mineral. Petrol.* **67**, 233 (1978).
25. M. Gascoyne, *Appl. Geochem* **1**, 199 (1986).
26. E. D. Ghent, M. Z. Stout, R. R. Parrish, in *Short Course on Heat, Metamorphism, and Tectonics*, E. G. Nisbet and C. M. R. Fowler, Eds. (Mineralogical Association of Canada, St. John's, 1988), vol. 14, pp. 155–188.
27. K. Mezger, C. M. Rawnsley, S. R. Bohlen, G. N. Hanson, *J. Geol.* **99**, 415 (1991).
28. For a description of $^{40}Ar/^{39}Ar$ analytical techniques at the University of Maine, see D. R. Lux [*Can. J. Earth Sci.* **23**, 21 (1986)]. Complete data tables for the R111 and R112 hornblendes are available on request.
29. P. Copeland, R. R. Parrish, T. M. Harrison, *Nature* **333**, 760 (1988).
30. U. Schärer, *Earth Planet. Sci Lett.* **67**, 191 (1984).
31. A description of analytical procedures for this facility may be found in R. R. Parrish, J. C. Roddick, W. D. Loveridge, R. W. Sullivan, in *Radiogenic Age and Isotopic Studies: Report 1* (Paper 87-2, Geological Survey of Canada, Ottawa, 1987), pp. 3–7.
32. P. K Zeitler and C P. Chamberlain, *Tectonics* **10**, 729 (1991)
33. R. R. Parrish, K. V. Hodges, A. Mactarlane, in *7th Himalaya-Tibet-Karakoram Workshop Abstracts*, M. P. Searle and P. J. Treloar, Eds. (Oxford University, Oxford, 1992), pp 67–68.
34. C. Ruppel, L. Royden, K. V. Hodges, *Tectonics* **7**, 947 (1988).
35. B. S. Hemingway, R. A. Robie, H. T. Evans, D. M. Kerrick, *Am. Mineral.* **76**, 1597 (1991).
36. A. B. Thompson, *Am. J. Sci.* **282**, 1567 (1982).
37. J. D. Clemens and V. J. Wall, *Can. Mineral.* **19**, 111 (1981).
38. D. Vielzeuf and J. R Holloway, *Contrib. Mineral. Petrol.* **98**, 257 (1988).
39 J. S. Stacey and J. D. Kramers, *Earth Planet. Sci. Lett.* **26**, 207 (1975).
40. Support for this research was provided by NSF grants EAR 85-13157 (B.C.B., K.V.H., and L.H.R.) and EAR 91-04291 (K.V.H.) and by the Geological Survey of Canada. We appreciate comments by two anonymous reviewers and B. Hanson on an earlier version of the manuscript.

6 July 1992; accepted 2 October 1992

# The Seismic Attenuation Structure of a Fast-Spreading Mid-Ocean Ridge

William S. D. Wilcock,* Sean C. Solomon,† G. M. Purdy, Douglas R. Toomey

**The two-dimensional P-wave attenuation structure of the axial crust of the East Pacific Rise was obtained from an inversion of waveform spectra collected during an active-source seismic tomography experiment. The structure shows that attenuation near the surface is high everywhere but decreases markedly within 1 to 3 kilometers of the rise axis. The near-axis variation is attributed to the thickening of the surface basalt layer and possibly to in situ changes in porosity related to hydrothermal circulation. High attenuation is also observed beneath the rise axis at depths ranging from about 2 kilometers (less than 1 kilometer beneath the axial magma lens) to the base of the crust. The levels of attenuation in this deeper region require at most only a small fraction of partial melt.**

Mid-ocean ridges dominate the Earth's global volcanic flux and have been the locus of formation of the crust covering two-thirds of the Earth's surface. Models of the generation and early evolution of oceanic crust must be constrained by observations of the structure and physical state of crustal material near mid-ocean ridge axes. Because seismic-wave propagation is affected by the composition, temperature, and porosity of the medium and by the presence of molten material, measurements of seismic properties are an important source of such constraints. Therefore, numerous experiments have measured the seismic velocity structure of mid-ocean ridges by such techniques as seismic refraction (*1*), multichannel reflection (*2, 3*) and expanding-spread (*4, 5*) profiling, and two- and three-dimensional (2-D and 3-D) tomography (*6–8*). A striking feature of the axial structure of fast-spreading ridges is a strong seismic reflector, at depths of 1 to 2 km, which has been interpreted as the roof of a thin magma lens or sill (*2, 9*). This feature is underlain by an extensive region of anomalously low velocities (*4–7*) that appears to extend to the base of the crust. In contrast, near-surface velocities on axis are markedly higher than elsewhere (*4–7, 10, 11*). One interpretation of the low-velocity region underlying the magma lens (*12*) is that it is a crystal mush zone extending downward to mid-crustal depths.

Few studies have addressed directly the attenuative properties of oceanic crust (*13, 14*), although measurements of attenuation provide complementary information on the state of crustal material. Spatial variations in the levels of seismic attenuation can exceed an order of magnitude, much larger than those observed for seismic velocities. Measurements of attenuation do carry large uncertainties. However, they are particularly sensitive to the characteristics of regions of high attenuation that result from high porosities or near-solidus temperatures. In this report, we derive a 2-D model of compressional-wave (P-wave) attenuation across the East Pacific Rise. Our results provide constraints on the evolution of shallow oceanic crust and on the volume of the axial region that contains a significant fraction of partial melt.

The data set for this study comes from an active seismic tomography experiment conducted at 9°30′N on the East Pacific Rise (Fig. 1). A total of 480 well-navigated explosive shots of uniform mass (54.5 kg), construction, and depth of detonation were recorded by 15 accurately located, ocean-bottom hydrophones and seismometers (*6*). The experiment configuration was designed to optimize the resolution of delay-time tomographic velocity models (*6*) within a 16 by 16 km area of crust centered on the rise axis. To obtain an accurate record of the source signature and to demonstrate its uniformity, we made several mid-water recordings of the explosive source. In addition, the instrument response has been carefully determined for all of the receivers (*15*).

Attenuation tomography relies on an inversion of measurements of the attenuation of waveforms $t^*$ for the quality factor $Q$ (a physical property whose reciprocal measures anelasticity) with the relation

W. S. D. Wilcock, Massachusetts Institute of Technology—Woods Hole Oceanographic Institution Joint Program in Oceanography, Cambridge, MA 02139.
S. C. Solomon, Department of Earth, Atmospheric, and Planetary Sciences, Massachusetts Institute of Technology, Cambridge, MA 02139.
G. M. Purdy, Department of Geology and Geophysics, Woods Hole Oceanographic Institution, Woods Hole, MA 02543.
D. R. Toomey, Department of Geological Sciences, University of Oregon, Eugene, OR 97403.

*Present address: Institute of Geophysics and Planetary Physics 0225, University of California at San Diego, La Jolla, CA 92093.
†Present address: Department of Terrestrial Magnetism, Carnegie Institution of Washington, Washington, DC 20015.